Atmos. Chem. Phys., 24, 6987–6999, 2024
https://doi.org/10.5194/acp-24-6987-2024

Atmospheric Chemistry and Physics
Open Access
EGU

Different formation pathways of nitrogen-containing organic compounds in aerosols and fog water in northern China

Wei Sun[1,2], Xiaodong Hu[3], Yuzhen Fu[4], Guohua Zhang[1,2], Yujiao Zhu[5], Xinfeng Wang[5], Caiqing Yan[5], Likun Xue[5], He Meng[6], Bin Jiang[1,2], Yuhong Liao[1,2], Xinming Wang[1,2], Ping'an Peng[1,2], and Xinhui Bi[1,2]

[1]State Key Laboratory of Organic Geochemistry and Guangdong Key Laboratory of Environmental Protection and Resources Utilization, Guangzhou Institute of Geochemistry, Chinese Academy of Sciences, Guangzhou, 510640, PR China
[2]Guangdong–Hong Kong–Macao Joint Laboratory for Environmental Pollution and Control, Guangzhou Institute of Geochemistry, Chinese Academy of Sciences, Guangzhou 510640, PR China
[3]Jiangmen Laboratory of Carbon Science and Technology, Hong Kong University of Science and Technology (Guangzhou), Jiangmen 529199, PR China
[4]Hainan Research Academy of Environmental Sciences, Haikou 571126, PR China
[5]Environment Research Institute, Shandong University, Qingdao 266237, PR China
[6]Qingdao Eco-environment Monitoring Center of Shandong Province, Qingdao 266003, PR China

Correspondence: Guohua Zhang (zhanggh@gig.ac.cn) and Xinhui Bi (bixh@gig.ac.cn)

Received: 10 January 2024 – Discussion started: 5 February 2024
Revised: 25 April 2024 – Accepted: 6 May 2024 – Published: 18 June 2024

Abstract. While aqueous-phase processing is known to contribute to the formation of nitrogen-containing organic compounds (NOCs), the specific pathways involved remain poorly understood. In this study, we aimed to characterize the NOCs present in both pre-fog aerosols and fog water collected at a suburban site in northern China. Fourier-transform ion cyclotron resonance mass spectrometry was utilized to analyze the molecular composition of NOCs in both negative and positive modes of electrospray ionization (ESI− and ESI+). In both pre-fog aerosols and fog water samples, NOCs constituted a significant portion, accounting for over 60 % of all assigned formulas in ESI− and more than 80 % in ESI+. By comparing the molecular composition of NOCs originating from biomass burning, coal combustion, and vehicle emissions, we identified that 72.3 % of NOCs in pre-fog aerosols were attributed to primary anthropogenic sources (pNOCs), while the remaining NOCs were categorized as secondary NOCs formed within the aerosols (saNOCs). Unique NOCs found in fog water were classified as secondary NOCs formed within the fog water (sfNOCs). Through a comprehensive "precursor–product pair" screening involving 39 reaction pathways, we observed that the nitration reaction, the amine pathway, and the intramolecular N-heterocycle pathway of NH_3 addition reactions contributed 43.6 %, 22.1 %, and 11.6 % of saNOCs, respectively. In contrast, these pathways contributed 26.8 %, 28.4 %, and 29.7 % of sfNOCs, respectively. This disparity in formation pathways is likely influenced by the diverse precursors, the aqueous acidity, and the gas-phase species partitioning. Correspondingly, saNOCs were found to contain a higher abundance of carbohydrate-like and highly oxygenated compounds with two nitrogen atoms compared to pNOCs. Conversely, sfNOCs exhibited a higher content of lipid-like compounds with fewer oxygen atoms. These results underscore the distinct secondary processes contributing to the diversity of NOCs in aerosols and fog water, which may lead to their different climate effects.

1 Introduction

Nitrogen-containing organic compounds (NOCs), predominantly comprising organonitrates, amines, amino acids, nitroaromatics, and nitrogen-heterocyclic compounds, have been extensively detected in aerosols, cloud/fog water, and rainwater (Altieri et al., 2012; X. Li et al., 2020; Wang et al., 2018; Feng et al., 2016; Leclair et al., 2012; Ditto et al., 2022). As essential contributors to the absorption of brown carbon, NOCs play a substantial role in influencing the radiative balance (Yang et al., 2022; Jimenez et al., 2022; Jiang et al., 2021; Huang et al., 2020). Certain NOCs, such as nitroaromatics, are classified as phytotoxins and suspected carcinogens (Harrison et al., 2005). Therefore, conducting an in-depth investigation into the characteristics, sources, and atmospheric processes of NOCs is imperative for understanding their climate and health effects.

Both primary emissions and secondary formation contribute to NOCs in the atmosphere. Benefiting from ultrahigh Fourier-transform ion cyclotron resonance mass spectrometry (FT-ICR MS), thousands of NOC molecules have been detected in primary anthropogenic sources, including biomass burning (BB), coal combustion (CC), and vehicle emission (VE) (Tang et al., 2020; Song et al., 2019, 2018, 2021). Meanwhile, aqueous-phase reactions have been identified as crucial pathways for the secondary formation of NOCs. Recent studies have revealed a positive relationship between NOCs and relative humidity or aerosol liquid water (X. Liu et al., 2023; Cai et al., 2023; Jiang et al., 2023) as well as the presence of abundant NOCs in cloud/fog water (Kim et al., 2019; Boone et al., 2015). Laboratory studies have highlighted two major pathways for NOC formation in the aqueous phase: (1) organic precursors can undergo nitration by the NO_2 radical or nitronium ion (NO_2^+), resulting in the formation of NOCs such as nitroaromatics (Kroflic et al., 2015; Vione et al., 2005), and (2) the reaction of carbonyl compounds (e.g., glyoxal and methylglyoxal) with ammonium and/or amines in the aqueous phase, known as Maillard reactions, can produce reduced NOCs, e.g., imidazoles (Jimenez et al., 2022; De Haan et al., 2009; Kua et al., 2011; De Haan et al., 2018). Both nitration and Maillard products, including dinitrophenols, methylnitrocatechols, and imidazoles, have been observed in aerosol liquid water and cloud/fog water (Lüttke et al., 1997; Harrison et al., 2005; Frka et al., 2016; Li et al., 2022; X. Liu et al., 2023; Lian et al., 2021). These reactions might be influenced by factors such as liquid water content (LWC) and pH of the aqueous phase (Lian et al., 2021; Vidovic et al., 2018). For instance, a low pH promotes the formation of 2,4-dinitrophenol via nitration (Vione et al., 2005), while inhibiting reactions between glyoxal and reduced nitrogen (Sedehi et al., 2013; Yang et al., 2024). Aerosol liquid water and fog water serve as crucial media for the aqueous-phase reactions of organics, characterized by significant differences in LWC and pH (Ervens et al., 2011; Blando and Turpin, 2000). However, due to the limited comprehensive studies of aqueous-phase processes in these two phases, the contribution of various formation pathways to secondary NOCs remains unclear.

In recent years, northern China has grappled with severe haze pollution, with anthropogenic sources like BB, CC, and VE identified as major contributors (J. Li et al., 2019; Li et al., 2023; M. Li et al., 2019; X. Li et al., 2019). Meanwhile, high relative humidity has been regarded as a significant driver of secondary pollution in this region (Xu et al., 2017; Kuang et al., 2020; J. Li et al., 2020). However, research on the understanding of NOCs at the molecular level remains limited (Wang et al., 2019). In this study, we collected pre-fog aerosols and fog water samples from a suburban site in northern China during a severe haze period. These samples were analyzed using FT-ICR MS coupled with electrospray ionization (ESI) in both negative and positive ionization modes. By employing this technique, up to 80 % of NOCs in samples can be detected (Cape et al., 2011; Jiang et al., 2022). Our study aimed to (1) identify primary NOCs originating from anthropogenic emissions and (2) explore the distinct formation pathways of NOCs in both pre-fog aerosols and fog water.

2 Materials and methods

2.1 Sample collection and pretreatment

The sampling site is situated in a suburban area of Qingdao, China (36.35° N, 120.68° E). It is surrounded by residential areas and roads. Aerosol and fog water samplers were installed on the roof of a four-story building. Detailed information regarding the environmental and meteorological conditions during the sampling campaign has been described elsewhere (Hu et al., 2022; Zhang et al., 2021).

During a severe haze episode lasting from 6 to 11 December 2019, the concentration of $PM_{2.5}$ soared to as high as 300 µg m^{-3} (Fig. S1 in the Supplement). On the morning of 10 December, a fog event occurred, characterized by visibility dropping below 100 m and relative humidity exceeding 90 %. This fog event persisted from approximately 06:30 to 11:20 local time (LT, UTC+8) (Fig. S1). During this period, two fog water samples (QDF1 and QDF2) were collected utilizing a Caltech Active Strand Cloud Water Collector, Version 2 (CASCC2). The CASCC2 operated at a flow rate of 5.8 m^3 min^{-1}, with a collection efficiency of 86 %. A blank sample for fog water was acquired by rinsing the CASCC2 during the sampling campaign. The collected fog water was filtered using polytetrafluoroethylene filters, and pH of the fog water was measured on-site using a pH meter (METTLER TOLEDO, Switzerland). Subsequently, the samples were preserved at −20 °C until further analysis.

Two aerosol samples collected on 8 and 9 December, prior to the fog event (labeled as pre-fog aerosols QDP1 and QDP2) were selected for comparative analysis with the fog water samples. Daily aerosol collection was conducted onto

quartz fiber filters with a radius of 45 mm (Pall, U.S.A.) using a $PM_{2.5}$ sampler (TH-150A, Wuhan Tianhong, China) at a flow rate of 100 L min^{-1}. To ensure the removal of any organic contaminants, the filters underwent pretreatment by baking in a muffle furnace at 450 °C for 4 h prior to sampling. Each sampling period lasted approximately 23.5 h, from 08:00 LT to around 07:30 LT the following day. Immediately after sampling, the filters were refrigerated at −20 °C for preservation. Additionally, a field blank was prepared and processed following the same procedure used for the samples.

For the FT-ICR MS analysis, one-eighth of the aerosol filters were cut into pieces and subjected to extraction with ultrapure water using ultrasonic agitation. The resulting extracts were then filtered through 0.22 µm polytetrafluoroethylene filters. Subsequently, water-soluble organic matter (WSOM) present in both fog water and water extracts from aerosols was isolated through a solid-phase extraction (SPE) process as described in our previous studies (Sun et al., 2024) and in Text S1. Briefly, the SPE cartridges (Strata-X, Phenomenex, USA) were initially pre-conditioned sequentially with isopropanol, acetonitrile, and methanol containing 0.1 % formic acid and ultrapure water containing 0.1 % formic acid. Then, samples with pH adjusted to 4.5 using formic acid were introduced to the cartridge. Inorganic salts were subsequently removed from the cartridges using ultrapure water containing 0.1 % formic acid. The cartridges were then subjected to freeze-drying, after which the analytes were eluted using 3 mL of acetonitrile / methanol / ultrapure water (45/45/10, $v:v:v$) at pH 10.4, with the pH being adjusted using ammonium hydroxide. The final eluent was dried using gentle nitrogen gas and subsequently frozen until analysis.

2.2 Instrumental analysis and data processing

The molecular composition of WSOM in fog water and aerosols was detected using an ESI source coupled with a 9.4-T solariX FT-ICR MS instrument (Bruker Daltonik GmbH, Bremen, Germany). Both negative and positive ionization modes of the ESI source were utilized. The samples were redissolved in 1 mL of methanol and injected into an ESI source at a flow rate of 200 µL h^{-1}. The mass range scanned was 100–800 Da. A total of 128 continuous 4M data FT-ICR transients were co-added to improve the signal-to-noise ratio and dynamic range. All mathematically possible formulas for ions with a signal-to-noise ratio greater than 10 were calculated, considering a mass tolerance of ±0.6 ppm. The maximum numbers of atoms for the formula calculator were set to 30 ^{12}C, 60 ^{1}H, 15 ^{16}O, 2 ^{14}N, 2 ^{32}S, 1 ^{13}C, 1 ^{18}O, and 1 ^{34}S for ESI− and one additional ^{23}Na for ESI+. Formulas assigned to isotopomers (i.e., ^{13}C, ^{18}O, or ^{34}S) were not discussed. The neutral molecular formula $C_cH_hO_oN_nS_s$ was achieved by adding H in ESI− or subtracting H or Na in ESI+. Note that there are other possible adducts, such as K, during the ionization in ESI+. However, the number of other adducts was very limited. Most of the current studies only considered the addition of H and Na in ESI+ (Sareen et al., 2016; Jiang et al., 2022). The other adducts were therefore not considered when we assigned formulas. Further screening was applied using the following criteria to exclude formulas not detected frequently in natural materials: $O/C \le 1.2$, $0.3 \le H/C \le 2.25$, $N/C \le 0.5$, $S/C \le 0.2$, $2C + 2 > H$, $C + 2 > O$, and obeying the N rule. Only ion peaks with intensities in the sample enhanced > 100 times higher than in the blank sample were retained for further analysis. More detailed information about the instrumental analysis can be found in our previous studies (Sun et al., 2021, 2023) and in Text S2. The double-bond equivalent (DBE) of each assigned formula $C_cH_hO_oN_nS_s$ was calculated as follows:

$$\mathrm{DBE} = (2c + 2 - h + n)/2. \quad (1)$$

The oxidation state of carbon atoms (OS_C) was calculated based on the equation described in Kroll et al. (2011) and Brege et al. (2018):

$$OS_C \approx 2 \times o/c - h/c - 5 \times n/c - 6 \times s/c. \quad (2)$$

For each sample, the average elemental ratios of oxygen, carbon, and hydrogen (i.e., O / C, H / C, etc.) and other characteristic parameters weighted by intensity were calculated as follows:

$$X = \Sigma\,(X_i \times \mathrm{Int}_i)\,/\,\Sigma \mathrm{Int}_i, \quad (3)$$

where X_i and Int_i represent the parameter and intensity, respectively, in the mass spectrum of each individual molecular formula, i.

Additionally, water-soluble ions in fog water were analyzed using an ion chromatograph (883 Basic IC plus, Metrohm, Switzerland).

3 Results and discussion

3.1 Profiles of molecular composition in pre-fog aerosol and fog water

The reconstructed mass spectra of ESI− and ESI+ FT-ICR MS for a typical sample is depicted in Fig. 1a. A total of 2659–3753 formulas in ESI− mode and 1695–2419 formulas in ESI+ mode were assigned for two pre-fog aerosol samples. Four molecular groups (CHO−, CHON−, CHOS−, and CHONS−) were categorized based on the elemental compositions of molecular formulas in ESI−, while three groups (CHO+, CHN+, and CHON+) were categorized in ESI+ mode. The fractions of their numbers and relative abundance (f_{RA}, normalized by the sum of intensity) are presented in Figs. 1b and S2. CHON represents the most abundant group in both modes. The numbers of NOCs (CHON−, CHONS−, CHN+, and CHON+) are 1697–2397

in ESI− and 1387–2039 in ESI+, comprising number fractions of 63.8 %–63.9 % (f_{RA} of 60.0 %–62.5 %) and 81.8 %–84.3 % (f_{RA} of 85.0 %–86.7 %) of all assigned formulas, respectively. The significant contribution of NOCs to organic aerosols has also been observed at rural (Jiang et al., 2023; Mao et al., 2022) and urban sites (Jang et al., 2020) in northern China during haze events.

Similar profiles were also observed in fog water. In total, 3903–3992 formulas in ESI− and 3011–3460 formulas in ESI+ mode were assigned to fog water samples, including 2551–2633 and 2477–2845 NOCs, respectively. NOCs constitute high number fractions of 65.0 %–66.0 % (f_{RA} of 69.7 %–75.0 %) and 82.2 %–82.3 % (f_{RA} of 84.1 %–85.7 %) of all formulas in ESI− and ESI+, respectively (Figs. 1b and S2). These fractions are higher than those observed in cloud water at Mt. Tai, where CHON accounts for 33 % and 63 % of all detected molecules in ESI− and ESI+ mode, respectively (Z. Liu et al., 2023). The high proportion of NOCs in this study may be related to enhanced emissions and subsequent secondary formation, as discussed in Sect. 3.2 and 3.3.

The molecular characteristics of NOCs, including oxidation states, unsaturation, and molecular weight, in pre-fog aerosols and fog water are presented in Table 1. Obviously, molecules in ESI− exhibit a higher oxidation state (O / C and OS_C), lower unsaturation (DBE), and lower molecular weight compared to those in ESI+. Interestingly, the H / C ratio of molecules in ESI− is lower than that in ESI+, seemingly an opposite trend of unsaturation with DBE. The plot of DBE versus H / C of CHON− and CHON+ clearly shows that CHON− usually has lower H / C than CHON+ at the same DBE value (Fig. S3). We note that CHON+ has a more abundant nitrogen atom content than CHON− (1.56 vs. 1.45 on average). The introduction of nitrogen into a molecule includes the possibility to form an N–C π bond and requires an additional H atom to fill the additional valence of nitrogen (Koch and Dittmar, 2006), which may lead to a higher average H / C of CHON+.

In general, the oxidation state of NOCs in fog water is similar to or slightly lower than that observed in aerosols. This trend may be partially attributed to different secondary formation pathways, as discussed in Sect. 3.3. The DBE values and molecular weight of CHON−, CHON+, and CHN+ in fog water are lower than those in pre-fog aerosols, but this is not the case for CHONS−. Certain CHONS− molecules with high DBE (9–11) and molecular weight (> 290) in fog water account for the higher average values (Fig. S4). The "precursor–product pair" analysis in Sect. 3.3 suggests that these molecules are likely formed through dehydrogenation, dehydration, and other aqueous-phase reactions involving the loss of hydrogen atoms in fog water.

3.2 Primary sources attribution of NOCs in pre-fog aerosols

Molecules detected in two ionization modes exhibit significant differences. A total of 826 NOCs formulas were common in both ionization modes in two pre-fog aerosol samples and 1050 in fog water samples, representing 22.2 % and 22.1 % of the total NOCs, respectively. The result indicates that the combination of ESI− and ESI+ will greatly expand the "event horizon" of the molecular compositions (Cooper et al., 2022). To ensure representativeness, molecules from both ionization modes in two samples will be combined to discuss the source and transformation of NOCs in the following text.

BB, CC, and VE were identified as the major sources of primary organic aerosols (> 80 %) in China (Wu et al., 2018) and significantly contribute to the haze events in northern China (X. Li et al., 2019). The study conducted at the same site also suggested significant residential combustion activities (Chen et al., 2023). Therefore, BB, CC, and VE likely serve as major primary sources at the sampling site. Some studies have characterized the molecular composition of BB (including both straw and wood), CC, and VE emissions. The primary NOCs in pre-fog aerosols were identified through comparison with datasets of the molecular composition of WSOM from BB (including corn, rice, and pine) and CC smoke detected by both ESI− and ESI+ coupled with FT-ICR MS and VE detected by ESI− FT-ICR MS (Song et al., 2018; Tang et al., 2020; Song et al., 2021). Then, NOCs in pre-fog aerosols were categorized into BB, CC, VE, and other sources. Similar methods have also been utilized for source attribution of the molecules detected in aerosols (Tang et al., 2022; Mao et al., 2022; Wang et al., 2019). The number of NOCs derived from BB, CC, and VE is 2298, 1557, and 547, accounting for 61.7 %, 41.8 %, and 14.7 % of the total NOCs, respectively. Some NOCs were assigned to more than one primary source. Mao et al. (2022) found that 28 % of CHON− and 32 % of CHON+ in aerosols collected at a rural site in North China Plain were common with CC emission (Mao et al., 2022), which is slightly lower than that in this study. Overall, the NOCs generated by primary anthropogenic sources (BB, CC, and VE; pNOCs) account for 72.3 % of the total NOCs in pre-fog aerosols. This suggests that anthropogenic emissions significantly contribute to the species richness of particulate NOCs during the haze event at this suburban site. Certainly, some other primary sources (e.g., cooking emission) might also contribute to NOCs but were not explicitly assigned in this study. This omission could introduce bias into the identification of pNOCs, which warrants more research on the molecular composition of these additional sources in the future.

The Van Krevelen (VK) diagram facilitates information retrieval from assigned molecules (Kim et al., 2003; Hockaday et al., 2009). In this study, NOC molecules from various sources were plotted on the VK diagram (Fig. 2), in which

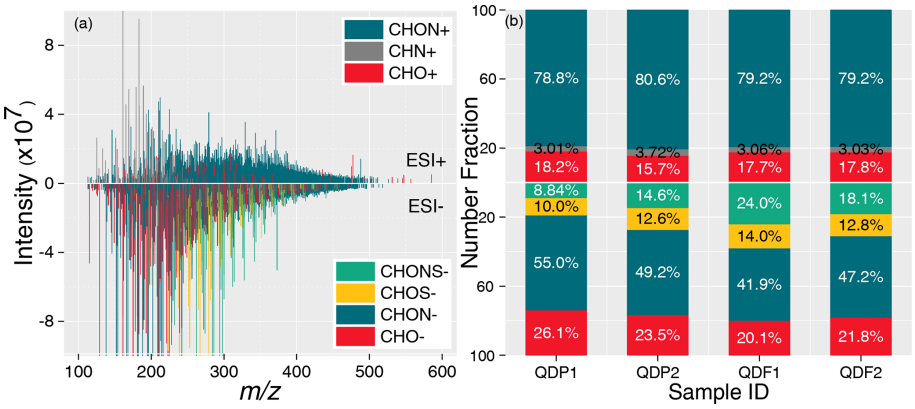

Figure 1. **(a)** The reconstructed mass spectra of a typical aerosol sample QDP1. The negative and positive values of the *y* axis represent the intensities of the ion peaks detected in ESI− and ESI+, respectively. **(b)** The number fraction (%) of each molecular group in ESI− and ESI+ mode.

Table 1. The ranges of the relative-abundance-weighted average values of the parameters (including O / C, OS_C, H / C, DBE, carbon number (No. C), and molecular weight (MW)).

		O / C	OS_C	H / C	DBE	No. C	MW
Pre-fog aerosol	CHON−	0.51–0.57	−0.66 to −0.67	1.05–1.17	6.42–6.54	10.75–11.81	242.2–277.7
	CHON+	0.31–0.34	−1.17 to −1.03	1.32–1.41	6.68–7.52	17.24–17.30	332.6–340.9
	CHONS−	0.81–0.86	−1.29 to −1.23	1.65–1.76	2.67–3.30	9.51–10.09	304.0–311.5
	CHN+	–	–	1.30–1.31	6.16–6.18	11.92–11.96	184.7–185.1
Fog water	CHON−	0.59–0.59	−0.77 to −0.73	0.98–1.02	5.82–5.96	8.47–9.19	207.8–222.9
	CHON+	0.31–0.31	−1.39 to −1.38	1.46–1.47	6.07–6.20	15.89–15.96	309.8–310.0
	CHONS−	0.78–0.81	−1.22 to −1.21	1.53–1.63	3.49–4.10	10.27–10.41	313.7–316.7
	CHN+	–	–	1.39–1.47	5.07–5.52	11.36–11.85	176.4–181.2

NOCs assigned to more than one source are labeled as mixed sources to avoid overlapping points. It is evident that pNOCs are mainly distributed in the lower left corner, where BB-generated pNOCs occupy the largest area. A previous study also identified the BB-generated NOCs in ambient aerosols by comparing them with laboratory combustion emissions. A similar distribution of these molecules in the VK plot was observed (Wang et al., 2019). Meanwhile, NOCs from other sources are located in the upper right area (Fig. 2). Consistently, the average O / C and H / C of pNOCs are significantly lower than those from other sources (Fig. S5). It should be noted that the deficiency of the dataset on the VE source in ESI+ may introduce uncertainty in assigning sources to molecules. However, our focus is on the overall trend of the secondary NOC formation process, rather than individual molecules. Importantly, ESI+ tends to ionize molecules with fewer oxygen and more hydrogen. Therefore, even with the inclusion of ESI+ molecules, the average O / C and H / C position of VE on the VK diagram would shift towards the upper left direction, without altering the relative position of "other sources" and pNOCs. NOCs from other sources have relatively higher O / C (0.65 ± 0.29), H / C (1.55 ± 0.42), and N / C (0.14 ± 0.07) compared to pNOCs (Fig. S5), resembling the characteristics of aged aerosols (Jiang et al., 2023). Therefore, it is reasonable to regard these NOCs from other sources as secondary NOCs.

3.3 The formation of secondary NOCs in pre-fog aerosols and fog water

To identify the formation pathways of secondary NOCs in pre-fog aerosol (saNOCs), the precursor–product pairs were screened from the formula list of pre-fog aerosols. A total of 39 reaction pathways were considered in the analysis (Table S1) (Lian et al., 2020; Z. Liu et al., 2023). These pathways can be classified into eight types, including the dealkyl group; oxygen addition; reaction of carboxylic acid; reaction of amine; reaction of the nitro/nitroso group; reaction of sulfur; NH_3 addition; and other reactions, covering oxidation, hydrolysis, fragmentation, and other typical aqueous-phase reactions. Note that some other reaction pathways, such as oligomerization, were not included in this study because their corresponding atomic variations within the molecules are too complex to describe using precursor–product pairs.

The primary molecules (i.e., molecules corresponding to BB, CC, or VE emissions, including both pNOCs and other

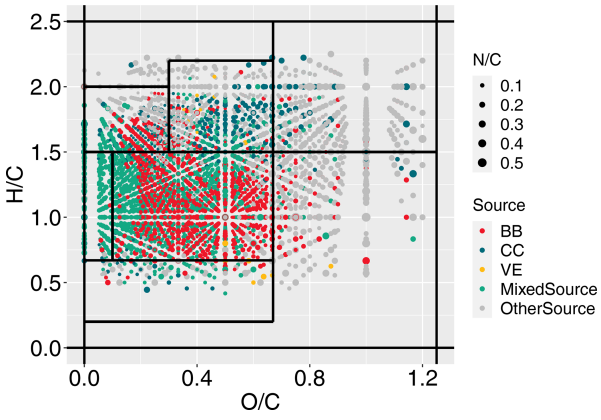

Figure 2. The Van Krevelen diagrams for NOCs from different sources (biomass burning, BB; coal combustion, CC; vehicle emission, VE; and other sources) in pre-fog aerosols. "MixedSource" in the plot represents the molecules that were assigned to at least two sources of BB, CC, and VE.

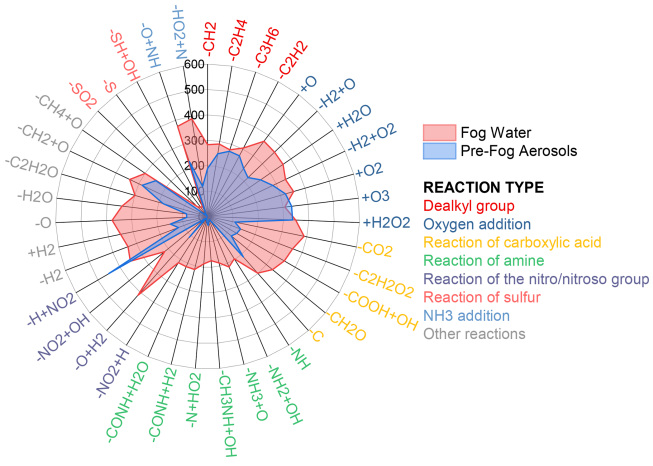

Figure 3. Radar plot of the links from precursors (primary molecules in aerosols and activated molecules in fog water) to products (saNOCs and sfNOCs) in pre-fog aerosols and fog water based on 39 reaction pathways. The *y* axis (0–600) in the plot represents the number of precursor–product pairs.

primary molecules) were considered to be precursors, while saNOCs were regarded as products. The products of 39 reaction pathways collectively account for 83 % of saNOCs, demonstrating their representativeness. Most of the reaction pathways involve the addition and subtraction of H, O, and C atoms to NOC molecules, such as the oxygen addition and dealkylation. Two types of formation pathways for saNOCs involving nitrogen addition on nitrogen-free or one-nitrogen molecules are nitration ($-H + NO_2$, corresponding to nitro substitution) and NH_3 addition. The NH_3 addition pathways include the amine pathway ($-O + NH$) and intramolecular N-heterocycle pathway ($-HO_2 + N$) of reactions between carbonyl compounds and ammonia, indexed as NH3Add1 and NH3Add2 in the following text, respectively (Table S1) (Z. Liu et al., 2023). As depicted in Fig. 3, three pathways (nitration, NH3Add1, and NH3Add2) produce 450, 228, and 120 saNOC products, accounting for 43.6 %, 22.1 %, and 11.6 % of all saNOCs, respectively, indicating nitration is the most important formation pathway of saNOCs. Nitration was widely identified in cloud and fog water (Harrison et al., 2005). However, a recent study showed that aqueous-phase reactions in aerosol liquid water were also important pathways for nitroaromatics formation (Jiang et al., 2023). Since the ESI− and ESI+ modes preferentially ionize acidic and basic functional groups, respectively (Song et al., 2021), the ratio of detected molecule numbers between ESI+ and ESI− ($MNR_{+/-}$) may reflect the relative contribution of functional groups of products to some extent. The $MNR_{+/-}$ of nitration products in saNOCs is 0.16, significantly lower than that of NH_3 addition products (0.85 and 0.76 for NH3Add1 and NH3Add2, respectively, as shown in Table S2). The result is consistent with the fact that NH_3 addition would introduce the reduced nitrogen into the molecules, making them more easily detectable by ESI+.

The pathways for the formation of secondary NOCs in fog water (sfNOCs) were assessed under the premise that fog droplets arise from the activation of pre-fog aerosols. Common molecules shared between fog water and pre-fog aerosols ($n = 4830$) were designated as activated molecules, while unique NOC molecules found solely in fog water ($n = 1315$) were identified as sfNOCs, following a similar approach as in a previous study (Z. Liu et al., 2023). The sfNOC molecules exhibit no significant differences in characteristic parameters (O / C and N / C) from activated NOC molecules, except for a slightly higher H / C ratio in the former (Figs. S6 and S7). These activated molecules and sfNOCs were subsequently considered to be precursors and products, respectively, in the precursor–product pair analysis. The products stemming from 39 reaction pathways collectively represent 92 % of sfNOCs. Illustrated in Fig. 3, the distribution of reaction pathways in fog water markedly differs from that observed in pre-fog aerosols. The contributions of these pathways in fog water are comparable to each other, except for the reaction of sulfur. For example, oxygen addition and carboxylic acid reactions lead to the addition and loss of oxygen atoms, respectively (Fig. 3 and Table S1). The contributions of these two pathways to sfNOCs are of similar magnitude (23.3 %–28.2 % and 22.7 %–29.6 %, respectively), potentially elucidating the similar O / C ratio between precursors and products in fog water. Upon scrutinizing the formation pathways of sfNOCs involving nitrogen addition, it becomes apparent that two NH_3 addition pathways are comparable to the nitration pathway in fog water. Nitration, NH3Add1, and NH3Add2 produce 352, 374, and 390 sfNOC products, constituting 26.8 %, 28.4 %, and 29.7 % of all sfNOCs, respectively. The $MNR_{+/-}$ of the sfNOCs generated by these three pathways is 0.25, 0.84, and 0.78, respec-

tively (Table S2), which is similar to that of saNOCs. Based on these analyses, it is evident that nitration plays a more pivotal role in the formation of NOCs in aerosols, while NH_3 addition prevails in fog water. Numerous laboratory studies have investigated the aqueous-phase reactions between carbonyls and reduced nitrogen (Ervens et al., 2011; Jimenez et al., 2022). However, field evidence of such reactions in the atmosphere remains scarce. Z. Liu et al. (2023) have suggested that NH_3 addition reactions are critical in the formation of reduced NOCs in cloud water at Mt. Tai (Z. Liu et al., 2023). The analogous finding in fog water from this study underscores the enhancement of NH_3 addition reactions in dilute aqueous phases.

It is important to note that some formulas regarded as precursors (primary molecules in aerosols and activated molecules in fog water) may also be formed through secondary processes. However, their formation would not necessarily increase the richness of organic composition. We primarily focused on the formation pathways of new molecular formulas that directly contribute to increasing chemical richness. Therefore, the formation of previously existing molecules was not considered.

3.4 Possible explanations for the different formation pathways of NOCs in aerosols and fog water

The different contributions of formation pathways to secondary NOCs in pre-fog aerosols and fog water may be linked to several factors, including the aqueous concentrations of nitrogen-containing species (e.g., NO_3^- and NH_4^+), the distribution of organic precursors, the properties of the aqueous phases (e.g., LWC and pH), and the gas-phase species partition.

First, the average NH_4^+ / NO_3^- ratios in terms of mass concentration in two fog water samples were found to be 0.45 and 0.57, respectively. The concentrations of water-soluble ions in pre-fog aerosols were not detected in this study. However, Zhang et al. (2021) collected fine ($< 1\,\mu m$) and coarse particulates ($> 1\,\mu m$) at the same site and observed NH_4^+ / NO_3^- ratios of 0.45–0.68 for PM_1 and 0.51–0.66 for $PM_{>1}$ collected on 8 and 9 December (corresponding to QDP1 and QDP2 in this study), which are close to or slightly higher than those in fog water (Zhang et al., 2021; Tang, 2021). Therefore, the disparate pathways of NOC formation cannot be solely attributed to variations of NH_4^+ and NO_3^- across the two phases.

Second, NH_3 addition reactions are exclusively viable on the carbonyl group, rendering them more selective than nitration. Precursors in pre-fog aerosols predominantly comprise primary molecules from BB, CC, and VE, with a low average O / C of 0.39. Conversely, those in fog water comprise more oxidized organics (O / C = 0.48 on average), encompassing both primary and secondary molecules formed in pre-fog aerosols, which may allow for the presence of more carbonyl groups (Figs. 2 and S6). Functional group identification is challenging in the formula list obtained via FT-ICR MS; however, carbonyls have been extensively detected in fog and cloud water at other sites (Ervens et al., 2013; van Pinxteren et al., 2005). Furthermore, a higher LWC in fog water compared with aerosols may facilitate the dissolution of carbonyl compounds (e.g., methylglyoxal) from the gas phase, augmenting their aqueous concentrations (T. Li et al., 2020). The heightened formation of imidazole, a typical product of carbonyls and ammonium/amine reactions, has also been observed in cloud droplets in southern China (Lian et al., 2021). Hence, it is reasonable to speculate that the divergent distributions of organic precursors, especially carbonyls, in the two phases may lead to distinct reaction pathways.

Third, the varying acidity levels in pre-fog aerosols and fog water likely provide another plausible explanation for the different contributions of various formation pathways to secondary NOCs. The pH value of fog water in this study was measured at 5.1, while the pH values of pre-fog aerosols (both PM_1 and $PM_{>1}$) were estimated to be less than 4.0 by the ISORROPIA-II model (Zhang et al., 2021; Tang, 2021). Such pH discrepancies may result in several-fold differences in reaction rates for nitration and NH_3 addition pathways. For instance, the formation rate of 2,4-dinitrophenol from the nitration of 4-nitrophenol at pH 4 is approximately 4.4 times higher than that at pH 5 (Vione et al., 2005), whereas the reaction rate between glyoxal and ammonium sulfate at pH 5 is approximately 15 times higher than that at pH 4 (IUPAC, 2017).

Finally, gas-phase nitrogen-containing species (NO_2, amines, and NH_3) may also influence NOC formation in aerosols and fog water through two pathways: (1) NOCs formed via gas-phase reactions partition into the condensed phase, and (2) gas-phase species partition into the condensed phase and subsequently participate in aqueous-phase NOC formation. While nitration can occur in the gas phase, the concentrations of NO_2 during pre-fog aerosol and fog water collection times were similar (51.5 and 53.0 ppb, respectively). Therefore, the variation in NO_2 levels cannot adequately explain the divergent formation pathways observed in the two phases. Furthermore, reactions between carbonyls and reduced nitrogen predominantly occur in the aqueous phase. Gas-phase NH_3 and amines may influence these reactions through the second pathway. Given the proximity of NH_4^+ / NO_3^- ratios in aerosols and fog water, variations in NH_3 or NH_4^+ concentrations are unlikely to account for differing reactions in the two phases. This discrepancy may be attributed to an excess of NH_3 in the reactions. However, previous studies have demonstrated that atmospheric amines primarily partition into cloud/fog water (Leng et al., 2015). Importantly, the formation of reduced nitrogen-containing compounds is more efficient in the presence of amines (Jimenez et al., 2022). Thus, gas-phase amines also have the potential to impact NOC formation through partitioning into fog water.

3.5 The impact of secondary processes on compositions of NOCs

To evaluate the impact of secondary processes on the molecular composition of NOCs, we classified NOCs into seven classes in the VK plot (Table S3) (Bianco et al., 2018). A heat map, generated based on these molecular classes, vividly illustrates the variations in the distribution of pNOCs, saNOCs, and sfNOCs (Fig. 4a). Notably, pNOCs in pre-fog aerosols predominantly consist of CRAM (carboxyl-rich alicyclic molecule)-like structures (61.4 %), whereas saNOCs exhibit an enrichment in carbohydrate-like compounds (28.3 % in saNOCs vs. 3.8 % in pNOCs) and highly oxygenated compounds (HOCs; 25.2 % in saNOCs vs. 4.6 % in pNOCs), indicative of the higher oxidation state and saturation of saNOCs. Conversely, sfNOCs display a significantly higher number fraction of lipid-like compounds (21.4 %) compared to pNOCs (8.0 %).

The divergent composition of saNOCs and sfNOCs results from distinct formation pathways. The nitration products in pre-fog aerosols are dominated by HOCs (37.5 %). Conversely, NH_3 addition reactions in pre-fog aerosols predominantly enhance aliphatic/peptide-like compounds (32.5 % and 26.1 % for NH3Add1 and NH3Add2, respectively, Fig. 4a). Obviously, the composition of nitration products is closely similar to that of all saNOCs, indicating a significant contribution of nitration in aerosols to the presence of highly oxygenated NOCs. The average relative humidity in this study during the pre-fog aerosol collection is 70 ± 14 % (Fig. S1). Based on ISORROPIA-II estimates, PM_1 samples collected on 8 and 9 December exhibited aerosol water contents of 33.9 and 22.3 $\mu g\,m^{-3}$, respectively (Tang, 2021). Such elevated relative humidity and liquid contents may favor the formation of HOCs in aerosol liquid water, as evidenced by observations of aqueous-phase formation of oxygenated organic aerosol during haze events in the North China Plain (Feng et al., 2022; Kuang et al., 2020; Xu et al., 2017). Applying the same method to fog water, NH3Add1 and NH3Add2 products enrich lipid-like NOCs (19.0 % and 21.2 %), whereas nitration products are dominated by HOCs (42.9 %). NH_3 addition products show a similar composition to all sfNOCs (Fig. 4a), illustrating that NH_3 addition plays an important role in shaping sfNOC composition.

Further subdivision of NOCs into different subclasses based on the distribution of characteristic elements (N, O, and S) can offer additional insights into molecular composition. The distribution of CHON molecule subclasses is depicted in Fig. 4b. pNOCs exhibit an approximate normal distribution with peaks at $–N_1O_7$ and $–N_2O_6$ for one- and two-nitrogen molecules ($–N_1$ and $–N_2$), respectively. In saNOCs, the fraction of $–N_1$ NOCs decreases, while that of $–N_2$ NOCs (e.g., $–N_2O_{5–7,10–12}$) increases. Conversely, sfNOCs display a lower content of oxygen atoms, with peaks at $–N_1O_5$ and $–N_2O_3$ (Fig. 4b). Nitration and NH_3 addition in pre-fog aerosols likely contribute to the augmentation of $–N_2O_{10–12}$ and $–N_2O_{5–7}$, respectively. The high ratio of O / N observed in these NOCs allows for the presence of $–NO_2$ or $–ONO_2$ functionalities (Leclair et al., 2012; Song et al., 2021). However, NH_3 addition products may encompass both reduced nitrogen and other oxidized functional groups. The surplus oxygen atoms may predominantly exist in the form of oxygen-containing functional groups, such as –OH and –COOH (Tang et al., 2022; Yang et al., 2023). In fog water, nitration and NH_3 addition mainly contribute to high- and low-oxygen-number molecules, respectively, with NH_3 addition products displaying a distribution similar to that of all the sfNOCs.

The heat map illustrating the distribution of CHONS is shown in Fig. S8, in which the same conclusion can be easily drawn, namely, that NH_3 addition reactions play a more significant role in shaping the composition of sfNOCs. In addition, the count of CHN in sfNOCs ($n = 29$) exceeds that in saNOCs ($n = 8$), which further underscores the heightened contribution from NH_3 addition in fog water.

4 Conclusions

A case study was conducted on the composition of NOCs in pre-fog aerosols and fog water at a suburban site in northern China during a winter haze episode. NOCs constitute over 60 % of all molecular formulas assigned by both ESI− and ESI+ modes coupled with FT-ICR MS, indicating a significant contribution of NOCs to the haze pollution. Primary anthropogenic emissions predominantly contribute to the species richness of NOCs in pre-fog aerosols, accounting for over 70 % of the number fraction, while the remaining fraction is attributed to secondary aqueous pathways. The nitration reaction plays a dominant role in secondary NOC formation in aerosols, while NH_3 addition pathways are more important in fog water. As a result, secondary NOCs in aerosols contain a high abundance of HOCs and carbohydrate compounds with two nitrogen atoms compared to primary NOCs. Differently, secondary NOCs formed in fog water are associated with increased lipid-like compounds, potentially containing more abundant reduced nitrogen. It is important to note that our findings may be specific to the observed conditions due to the limited sample size. Therefore, conducting more representative research that includes a broader range of samples under different environmental conditions is necessary in the future. Nevertheless, this study highlights that reactions occurring in aerosols and fog water yield distinct secondary NOC compositions. Particularly noteworthy is the identification of NH_3 addition and corresponding reduced NOC formation in fog water. This phenomenon has not been widely recognized since limited studies have utilized ESI+ to capture reduced NOCs in cloud and fog water (Z. Liu et al., 2023). Both oxidized NOCs (e.g., nitrophenols) and reduced NOCs (e.g., imidazole) constitute the brown carbon component. However, their maximum ab-

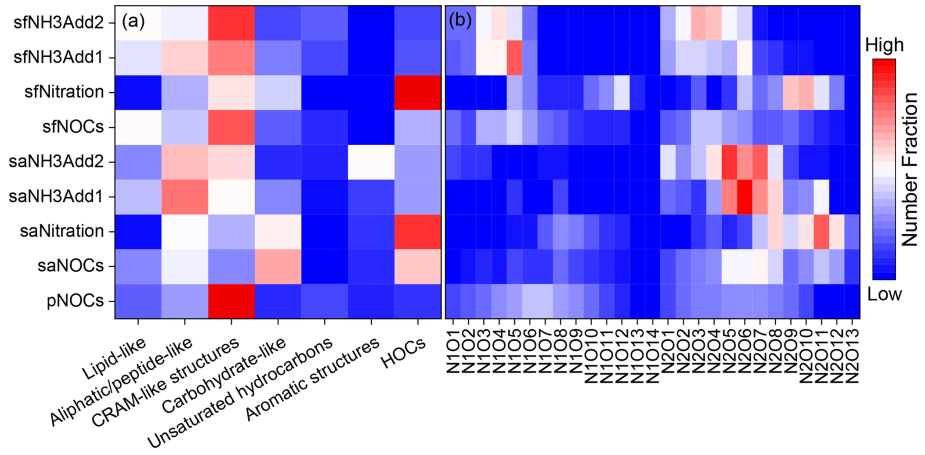

Figure 4. The heat map of seven classes of NOCs divided by O / C and H / C **(a)** and subclasses of CHON divided by the number of N and O atoms in pNOCs, all saNOCs, all sfNOCs, and NOCs formed by nitration and NH_3 addition **(b)**.

sorption wavelengths differ, potentially resulting in distinct climate effects. Considering that secondary NOCs formed in the aqueous phase may contribute to secondary organic aerosols, gaining a deeper understanding of their aqueous-phase formation processes will be crucial for better assessing their climate effects.

Data availability. The concentrations of water-soluble inorganic ions in aerosols were obtained from Tang (2021, https://doi.org/10.5281/zenodo.5774638). The kinetic data of the reaction between glyoxal and ammonium sulfate were obtained from https://iupac.aeris-data.fr (IUPAC, 2017). The organic molecular compositions of fog water and aerosols are available from the corresponding author upon request.

Supplement. The Supplement includes two texts (Texts S1–S2), eight figures (Figs. S1–S8), and three tables (Tables S1–S3) related to the paper. The supplement related to this article is available online at: https://doi.org/10.5194/acp-24-6987-2024-supplement.

Author contributions. XB and GZ designed the research with input from XinmW and PP. WS, XH, and YF collected samples. WS and BJ carried out the sample pretreatment and instrumental analysis under the guidance of YL. WS processed data and wrote the manuscript. XB and GZ edited the manuscript. LX, CY, XinfW, YZ, and HM had an active role in supporting the sampling work. All authors contributed to the discussions of the results and refinement of the manuscript.

Competing interests. The contact author has declared that none of the authors has any competing interests.

Disclaimer. Publisher's note: Copernicus Publications remains neutral with regard to jurisdictional claims made in the text, published maps, institutional affiliations, or any other geographical representation in this paper. While Copernicus Publications makes every effort to include appropriate place names, the final responsibility lies with the authors.

Financial support. This research has been supported by the National Key Research and Development Program of China (grant nos. 2022YFC3701103 and 2023YFC3710100), the Postdoctoral Fellowship Program of the CPSF (grant no. GZC20232683), the National Natural Science Foundation of China (grant nos. 42222705, 42130611, and 42207120), the Youth Innovation Promotion Association of the Chinese Academy of Sciences (grant no. 2021354), and the Guangdong Provincial Applied Science and Technology Research and Development Program (grant no. 2023B1212060049).

Review statement. This paper was edited by Qiang Zhang and reviewed by two anonymous referees.

References

Altieri, K. E., Hastings, M. G., Peters, A. J., and Sigman, D. M.: Molecular characterization of water soluble organic nitrogen in marine rainwater by ultra-high resolution electrospray ionization mass spectrometry, Atmos. Chem. Phys., 12, 3557–3571, https://doi.org/10.5194/acp-12-3557-2012, 2012.

Bianco, A., Deguillaume, L., Vaitilingom, M., Nicol, E., Baray, J. L., Chaumerliac, N., and Bridoux, M.: Molecular Characterization of Cloud Water Samples Collected at the Puy de Dome (France) by Fourier Transform Ion Cyclotron Resonance Mass Spectrometry, Environ. Sci. Technol., 52, 10275–10285, https://doi.org/10.1021/acs.est.8b01964, 2018.

Blando, J. D. and Turpin, B. J.: Secondary organic aerosol formation in cloud and fog droplets: a literature eval-

uation of plausibility, Atmos. Environ., 34, 1623–1632, https://doi.org/10.1016/S1352-2310(99)00392-1, 2000.

Boone, E. J., Laskin, A., Laskin, J., Wirth, C., Shepson, P. B., Stirm, B. H., and Pratt, K. A.: Aqueous Processing of Atmospheric Organic Particles in Cloud Water Collected via Aircraft Sampling, Environ. Sci. Technol., 49, 8523–8530, https://doi.org/10.1021/acs.est.5b01639, 2015.

Brege, M., Paglione, M., Gilardoni, S., Decesari, S., Facchini, M. C., and Mazzoleni, L. R.: Molecular insights on aging and aqueous-phase processing from ambient biomass burning emissions-influenced Po Valley fog and aerosol, Atmos. Chem. Phys., 18, 13197–13214, https://doi.org/10.5194/acp-18-13197-2018, 2018.

Cai, Y., Ye, C., Chen, W., Hu, W., Song, W., Peng, Y., Huang, S., Qi, J., Wang, S., Wang, C., Wu, C., Wang, Z., Wang, B., Huang, X., He, L., Gligorovski, S., Yuan, B., Shao, M., and Wang, X.: The important contribution of secondary formation and biomass burning to oxidized organic nitrogen (OON) in a polluted urban area: insights from in situ measurements of a chemical ionization mass spectrometer (CIMS), Atmos. Chem. Phys., 23, 8855–8877, https://doi.org/10.5194/acp-23-8855-2023, 2023.

Cape, J. N., Cornell, S. E., Jickells, T. D., and Nemitz, E.: Organic nitrogen in the atmosphere – Where does it come from? A review of sources and methods, Atmos. Res., 102, 30–48, https://doi.org/10.1016/j.atmosres.2011.07.009, 2011.

Chen, H., Yan, C., Fu, Q., Wang, X., Tang, J., Jiang, B., Sun, H., Luan, T., Yang, Q., Zhao, Q., Li, J., Zhang, G., Zheng, M., Zhou, X., Chen, B., Du, L., Zhou, R., Zhou, T., and Xue, L.: Optical properties and molecular composition of wintertime atmospheric water-soluble organic carbon in different coastal cities of eastern China, Sci. Total Environ., 892, 164702, https://doi.org/10.1016/j.scitotenv.2023.164702, 2023.

Cooper, W. T., Chanton, J. C., D'Andrilli, J., Hodgkins, S. B., Podgorski, D. C., Stenson, A. C., Tfaily, M. M., and Wilson, R. M.: A History of Molecular Level Analysis of Natural Organic Matter by FTICR Mass Spectrometry and The Paradigm Shift in Organic Geochemistry, Mass. Spectrom. Rev., 41, 215–239, https://doi.org/10.1002/mas.21663, 2022.

De Haan, D. O., Corrigan, A. L., Smith, K. W., Stroik, D. R., Turley, J. J., Lee, F. E., Tolbert, M. A., Jimenez, J. L., Cordova, K. E., and Ferrell, G. R.: Secondary Organic Aerosol-Forming Reactions of Glyoxal with Amino Acids, Environ. Sci. Technol., 43, 2818–2824, https://doi.org/10.1021/es803534f, 2009.

De Haan, D. O., Tapavicza, E., Riva, M., Cui, T., Surratt, J. D., Smith, A. C., Jordan, M. C., Nilakantan, S., Almodovar, M., Stewart, T. N., de Loera, A., De Haan, A. C., Cazaunau, M., Gratien, A., Pangui, E., and Doussin, J. F.: Nitrogen-Containing, Light-Absorbing Oligomers Produced in Aerosol Particles Exposed to Methylglyoxal, Photolysis, and Cloud Cycling, Environ. Sci. Technol., 52, 4061–4071, https://doi.org/10.1021/acs.est.7b06105, 2018.

Ditto, J. C., Machesky, J., and Gentner, D. R.: Analysis of reduced and oxidized nitrogen-containing organic compounds at a coastal site in summer and winter, Atmos. Chem. Phys., 22, 3045–3065, https://doi.org/10.5194/acp-22-3045-2022, 2022.

Ervens, B., Turpin, B. J., and Weber, R. J.: Secondary organic aerosol formation in cloud droplets and aqueous particles (aqSOA): a review of laboratory, field and model studies, Atmos. Chem. Phys., 11, 11069–11102, https://doi.org/10.5194/acp-11-11069-2011, 2011.

Ervens, B., Wang, Y., Eagar, J., Leaitch, W. R., Macdonald, A. M., Valsaraj, K. T., and Herckes, P.: Dissolved organic carbon (DOC) and select aldehydes in cloud and fog water: the role of the aqueous phase in impacting trace gas budgets, Atmos. Chem. Phys., 13, 5117–5135, https://doi.org/10.5194/acp-13-5117-2013, 2013.

Feng, S., Zhang, L., Wang, S., Nadykto, A. B., Xu, Y., Shi, Q., Jiang, B., and Qian, W.: Characterization of dissolved organic nitrogen in wet deposition from Lake Erhai basin by using ultrahigh resolution FT-ICR mass spectrometry, Chemosphere, 156, 438–445, https://doi.org/10.1016/j.chemosphere.2016.04.039, 2016.

Feng, Z., Liu, Y., Zheng, F., Yan, C., Fu, P., Zhang, Y., Lian, C., Wang, W., Cai, J., Du, W., Chu, B., Wang, Y., Kangasluoma, J., Bianchi, F., Petäjä, T., and Kulmala, M.: Highly oxidized organic aerosols in Beijing: Possible contribution of aqueous-phase chemistry, Atmos. Environ., 273, 118971, https://doi.org/10.1016/j.atmosenv.2022.118971, 2022.

Frka, S., Sala, M., Kroflic, A., Hus, M., Cusak, A., and Grgic, I.: Quantum Chemical Calculations Resolved Identification of Methylnitrocatechols in Atmospheric Aerosols, Environ. Sci. Technol., 50, 5526–5535, https://doi.org/10.1021/acs.est.6b00823, 2016.

Harrison, M. A. J., Barra, S., Borghesi, D., Vione, D., Arsene, C., and Iulian Olariu, R.: Nitrated phenols in the atmosphere: a review, Atmos. Environ., 39, 231–248, https://doi.org/10.1016/j.atmosenv.2004.09.044, 2005.

Hockaday, W. C., Purcell, J. M., Marshall, A. G., Baldock, J. A., and Hatcher, P. G.: Electrospray and photoionization mass spectrometry for the characterization of organic matter in natural waters: a qualitative assessment, Limno. Oceanogr.-Meth., 7, 81–95, https://doi.org/10.4319/lom.2009.7.81, 2009.

Hu, X., Guo, Z., Sun, W., Lian, X., Fu, Y., Meng, H., Zhu, Y., Zhang, G., Wang, X., Xue, L., Bi, X., Wang, X., and Peng, P. a.: Atmospheric Processing of Particulate Imidazole Compounds Driven by Photochemistry, Environ. Sci. Technol. Lett., 9, 265–271, https://doi.org/10.1021/acs.estlett.2c00029, 2022.

Huang, R. J., Yang, L., Shen, J., Yuan, W., Gong, Y., Guo, J., Cao, W., Duan, J., Ni, H., Zhu, C., Dai, W., Li, Y., Chen, Y., Chen, Q., Wu, Y., Zhang, R., Dusek, U., O'Dowd, C., and Hoffmann, T.: Water-Insoluble Organics Dominate Brown Carbon in Wintertime Urban Aerosol of China: Chemical Characteristics and Optical Properties, Environ. Sci. Technol., 54, 7836–7847, https://doi.org/10.1021/acs.est.0c01149, 2020.

IUPAC: IUPAC Task Group on Atmospheric Chemical Kinetic Data Evaluation, IUPAC [data set], https://iupac.aeris-data.fr (last access: 10 January 2024), 2017.

Jang, K. S., Choi, M., Park, M., Park, M. H., Kim, Y. H., Seo, J., Wang, Y., Hu, M., Bae, M. S., and Park, K.: Assessment of PM(2.5)-bound nitrogen-containing organic compounds (NOCs) during winter at urban sites in China and Korea, Environ. Pollut., 265, 114870, https://doi.org/10.1016/j.envpol.2020.114870, 2020.

Jiang, H., Li, J., Sun, R., Tian, C., Tang, J., Jiang, B., Liao, Y., Chen, C. E., and Zhang, G.: Molecular Dynamics and Light Absorption Properties of Atmospheric Dissolved Organic Matter, Environ. Sci. Technol., 55, 10268–10279, https://doi.org/10.1021/acs.est.1c01770, 2021.

Jiang, H., Li, J., Tang, J., Zhao, S., Chen, Y., Tian, C., Zhang, X., Jiang, B., Liao, Y., and Zhang, G.: Factors Influencing the Molecular Compositions and Distributions of Atmospheric Nitrogen-Containing Compounds, J. Geophys. Res.-Atmos., 127, e2021JD036284, https://doi.org/10.1029/2021jd036284, 2022.

Jiang, H., Cai, J., Feng, X., Chen, Y., Wang, L., Jiang, B., Liao, Y., Li, J., Zhang, G., Mu, Y., and Chen, J.: Aqueous-Phase Reactions of Anthropogenic Emissions Lead to the High Chemodiversity of Atmospheric Nitrogen-Containing Compounds during the Haze Event, Environ. Sci. Technol., 57, 16500–16511, https://doi.org/10.1021/acs.est.3c06648, 2023.

Jimenez, N. G., Sharp, K. D., Gramyk, T., Ugland, D. Z., Tran, M.-K., Rojas, A., Rafla, M. A., Stewart, D., Galloway, M. M., Lin, P., Laskin, A., Cazaunau, M., Pangui, E., Doussin, J.-F., and De Haan, D. O.: Radical-Initiated Brown Carbon Formation in Sunlit Carbonyl–Amine–Ammonium Sulfate Mixtures and Aqueous Aerosol Particles, ACS Earth Space Chem., 6, 228–238, https://doi.org/10.1021/acsearthspacechem.1c00395, 2022.

Kim, H., Collier, S., Ge, X., Xu, J., Sun, Y., Jiang, W., Wang, Y., Herckes, P., and Zhang, Q.: Chemical processing of water-soluble species and formation of secondary organic aerosol in fogs, Atmos. Environ., 200, 158–166, https://doi.org/10.1016/j.atmosenv.2018.11.062, 2019.

Kim, S., Kramer, R. W., and Hatcher, P. G.: Graphical Method for Analysis of Ultrahigh-Resolution Broadband Mass Spectra of Natural Organic Matter, the Van Krevelen Diagram, Anal. Chem., 75, 5336–5344, https://doi.org/10.1021/ac034415p, 2003.

Koch, B. P. and Dittmar, T.: From mass to structure: an aromaticity index for high-resolution mass data of natural organic matter, Rapid Commun. Mass Sp., 20, 926–932, https://doi.org/10.1002/rcm.2386, 2006.

Kroflic, A., Grilc, M., and Grgic, I.: Does toxicity of aromatic pollutants increase under remote atmospheric conditions?, Sci. Rep., 5, 8859, https://doi.org/10.1038/srep08859, 2015.

Kroll, J. H., Donahue, N. M., Jimenez, J. L., Kessler, S. H., Canagaratna, M. R., Wilson, K. R., Altieri, K. E., Mazzoleni, L. R., Wozniak, A. S., Bluhm, H., Mysak, E. R., Smith, J. D., Kolb, C. E., and Worsnop, D. R.: Carbon oxidation state as a metric for describing the chemistry of atmospheric organic aerosol, Nat. Chem., 3, 133–139, https://doi.org/10.1038/nchem.948, 2011.

Kua, J., Krizner, H. E., and De Haan, D. O.: Thermodynamics and kinetics of imidazole formation from glyoxal, methylamine, and formaldehyde: a computational study, J. Phys. Chem. A, 115, 1667–1675, https://doi.org/10.1021/jp111527x, 2011.

Kuang, Y., He, Y., Xu, W., Yuan, B., Zhang, G., Ma, Z., Wu, C., Wang, C., Wang, S., Zhang, S., Tao, J., Ma, N., Su, H., Cheng, Y., Shao, M., and Sun, Y.: Photochemical Aqueous-Phase Reactions Induce Rapid Daytime Formation of Oxygenated Organic Aerosol on the North China Plain, Environ. Sci. Technol., 54, 3849–3860, https://doi.org/10.1021/acs.est.9b06836, 2020.

Leclair, J. P., Collett, J. L., and Mazzoleni, L. R.: Fragmentation analysis of water-soluble atmospheric organic matter using ultrahigh-resolution FT-ICR mass spectrometry, Environ. Sci. Technol., 46, 4312–4322, https://doi.org/10.1021/es203509b, 2012.

Leng, C., Kish, J. D., Roberts, J. E., Dwebi, I., Chon, N., and Liu, Y.: Temperature-Dependent Henry's Law Constants of Atmospheric Amines, J. Phys. Chem. A, 119, 8884–8891, https://doi.org/10.1021/acs.jpca.5b05174, 2015.

Li, D., Wu, C., Zhang, S., Lei, Y., Lv, S., Du, W., Liu, S., Zhang, F., Liu, X., Liu, L., Meng, J., Wang, Y., Gao, J., and Wang, G.: Significant coal combustion contribution to water-soluble brown carbon during winter in Xingtai, China: Optical properties and sources, J. Environ. Sci. (China), 124, 892–900, https://doi.org/10.1016/j.jes.2022.02.026, 2023.

Li, J., Wang, G., Zhang, Q., Li, J., Wu, C., Jiang, W., Zhu, T., and Zeng, L.: Molecular characteristics and diurnal variations of organic aerosols at a rural site in the North China Plain with implications for the influence of regional biomass burning, Atmos. Chem. Phys., 19, 10481–10496, https://doi.org/10.5194/acp-19-10481-2019, 2019.

Li, J., Liu, Z., Gao, W., Tang, G., Hu, B., Ma, Z., and Wang, Y.: Insight into the formation and evolution of secondary organic aerosol in the megacity of Beijing, China, Atmos. Environ., 220, 117070, https://doi.org/10.1016/j.atmosenv.2019.117070, 2020.

Li, M., Fan, X., Zhu, M., Zou, C., Song, J., Wei, S., Jia, W., and Peng, P.: Abundance and Light Absorption Properties of Brown Carbon Emitted from Residential Coal Combustion in China, Environ. Sci. Technol., 53, 595–603, https://doi.org/10.1021/acs.est.8b05630, 2019.

Li, M., Wang, X., Zhao, Y., Du, P., Li, H., Li, J., Shen, H., Liu, Z., Jiang, Y., Chen, J., Bi, Y., Zhao, Y., Xue, L., Wang, Y., Chen, J., and Wang, W.: Atmospheric Nitrated Phenolic Compounds in Particle, Gaseous, and Aqueous Phases During Cloud Events at a Mountain Site in North China: Distribution Characteristics and Aqueous-Phase Formation, J. Geophys. Res.-Atmos., 127, e2022JD037130, https://doi.org/10.1029/2022jd037130, 2022.

Li, T., Wang, Z., Wang, Y., Wu, C., Liang, Y., Xia, M., Yu, C., Yun, H., Wang, W., Wang, Y., Guo, J., Herrmann, H., and Wang, T.: Chemical characteristics of cloud water and the impacts on aerosol properties at a subtropical mountain site in Hong Kong SAR, Atmos. Chem. Phys., 20, 391–407, https://doi.org/10.5194/acp-20-391-2020, 2020.

Li, X., Jiang, L., Bai, Y., Yang, Y., Liu, S., Chen, X., Xu, J., Liu, Y., Wang, Y., Guo, X., Wang, Y., and Wang, G.: Wintertime aerosol chemistry in Beijing during haze period: Significant contribution from secondary formation and biomass burning emission, Atmos. Res., 218, 25–33, https://doi.org/10.1016/j.atmosres.2018.10.010, 2019.

Li, X., Wang, Y., Hu, M., Tan, T., Li, M., Wu, Z., Chen, S., and Tang, X.: Characterizing chemical composition and light absorption of nitroaromatic compounds in the winter of Beijing, Atmos. Environ., 237, 117712, https://doi.org/10.1016/j.atmosenv.2020.117712, 2020.

Lian, L., Yan, S., Zhou, H., and Song, W.: Overview of the Phototransformation of Wastewater Effluents by High-Resolution Mass Spectrometry, Environ. Sci. Technol., 54, 1816–1826, https://doi.org/10.1021/acs.est.9b04669, 2020.

Lian, X., Zhang, G., Yang, Y., Lin, Q., Fu, Y., Jiang, F., Peng, L., Hu, X., Chen, D., Wang, X., Peng, P. a., Sheng, G., and Bi, X.: Evidence for the Formation of Imidazole from Carbonyls and Reduced Nitrogen Species at the Individual Particle Level in the Ambient Atmosphere, Environ. Sci. Technol. Lett., 8, 9–15, https://doi.org/10.1021/acs.estlett.0c00722, 2021.

Liu, X., Wang, H., Wang, F., Lv, S., Wu, C., Zhao, Y., Zhang, S., Liu, S., Xu, X., Lei, Y., and Wang, G.: Secondary Formation of

Atmospheric Brown Carbon in China Haze: Implication for an Enhancing Role of Ammonia, Environ. Sci. Technol., 57, 11163–11172, https://doi.org/10.1021/acs.est.3c03948, 2023.

Liu, Z., Zhu, B., Zhu, C., Ruan, T., Li, J., Chen, H., Li, Q., Wang, X., Wang, L., Mu, Y., Collett, J., George, C., Wang, Y., Wang, X., Su, J., Yu, S., Mellouki, A., Chen, J., and Jiang, G.: Abundant nitrogenous secondary organic aerosol formation accelerated by cloud processing, iScience, 26, 108317, https://doi.org/10.1016/j.isci.2023.108317, 2023.

Lüttke, J., Scheer, V., Levsen, K., Wünsch, G., Cape, J. N., Hargreaves, K. J., Storeton-West, R. L., Acker, K., Wieprecht, W., and Jones, B.: Occurrence and formation of nitrated phenols in and out of cloud, Atmos. Environ., 2637–2648, https://doi.org/10.1016/S1352-2310(96)00229-4, 1997.

Mao, J., Cheng, Y., Bai, Z., Zhang, W., Zhang, L., Chen, H., Wang, L., Li, L., and Chen, J.: Molecular characterization of nitrogen-containing organic compounds in the winter North China Plain, Sci. Total Environ., 838, 156189, https://doi.org/10.1016/j.scitotenv.2022.156189, 2022.

Sareen, N., Carlton, A. G., Surratt, J. D., Gold, A., Lee, B., Lopez-Hilfiker, F. D., Mohr, C., Thornton, J. A., Zhang, Z., Lim, Y. B., and Turpin, B. J.: Identifying precursors and aqueous organic aerosol formation pathways during the SOAS campaign, Atmos. Chem. Phys., 16, 14409–14420, https://doi.org/10.5194/acp-16-14409-2016, 2016.

Sedehi, N., Takano, H., Blasic, V. A., Sullivan, K. A., and De Haan, D. O.: Temperature- and pH-dependent aqueous-phase kinetics of the reactions of glyoxal and methylglyoxal with atmospheric amines and ammonium sulfate, Atmos. Environ., 77, 656–663, https://doi.org/10.1016/j.atmosenv.2013.05.070, 2013.

Song, J., Li, M., Jiang, B., Wei, S., Fan, X., and Peng, P.: Molecular Characterization of Water-Soluble Humic like Substances in Smoke Particles Emitted from Combustion of Biomass Materials and Coal Using Ultrahigh-Resolution Electrospray Ionization Fourier Transform Ion Cyclotron Resonance Mass Spectrometry, Environ. Sci. Technol., 52, 2575–2585, https://doi.org/10.1021/acs.est.7b06126, 2018.

Song, J., Li, M., Fan, X., Zou, C., Zhu, M., Jiang, B., Yu, Z., Jia, W., Liao, Y., and Peng, P.: Molecular Characterization of Water- and Methanol-Soluble Organic Compounds Emitted from Residential Coal Combustion Using Ultrahigh-Resolution Electrospray Ionization Fourier Transform Ion Cyclotron Resonance Mass Spectrometry, Environ. Sci. Technol., 53, 13607–13617, https://doi.org/10.1021/acs.est.9b04331, 2019.

Song, J., Li, M., Zou, C., Cao, T., Fan, X., Jiang, B., Yu, Z., Jia, W., and Peng, P.: Molecular Characterization of Nitrogen-Containing Compounds in Humic-like Substances Emitted from Biomass Burning and Coal Combustion, Environ. Sci. Technol., 56, 119–130, https://doi.org/10.1021/acs.est.1c04451, 2021.

Sun, W., Fu, Y., Zhang, G., Yang, Y., Jiang, F., Lian, X., Jiang, B., Liao, Y., Bi, X., Chen, D., Chen, J., Wang, X., Ou, J., Peng, P., and Sheng, G.: Measurement report: Molecular characteristics of cloud water in southern China and insights into aqueous-phase processes from Fourier transform ion cyclotron resonance mass spectrometry, Atmos. Chem. Phys., 21, 16631–16644, https://doi.org/10.5194/acp-21-16631-2021, 2021.

Sun, W., Guo, Z., Peng, X., Lin, J., Fu, Y., Yang, Y., Zhang, G., Jiang, B., Liao, Y., Chen, D., Wang, X., and Bi, X.: Molecular characteristics, sources and transformation of water-insoluble organic matter in cloud water, Environ. Pollut., 325, 121430, https://doi.org/10.1016/j.envpol.2023.121430, 2023.

Sun, W., Zhang, G., Guo, Z., Fu, Y., Peng, X., Yang, Y., Hu, X., Lin, J., Jiang, F., Jiang, B., Liao, Y., Chen, D., Chen, J., Ou, J., Wang, X., Peng, P. A., and Bi, X.: Formation of In-Cloud Aqueous-Phase Secondary Organic Matter and Related Characteristic Molecules, J. Geophys. Res.-Atmos., 129, e2023JD040355, https://doi.org/10.1029/2023jd040355, 2024.

Tang, J., Li, J., Su, T., Han, Y., Mo, Y., Jiang, H., Cui, M., Jiang, B., Chen, Y., Tang, J., Song, J., Peng, P., and Zhang, G.: Molecular compositions and optical properties of dissolved brown carbon in biomass burning, coal combustion, and vehicle emission aerosols illuminated by excitation–emission matrix spectroscopy and Fourier transform ion cyclotron resonance mass spectrometry analysis, Atmos. Chem. Phys., 20, 2513–2532, https://doi.org/10.5194/acp-20-2513-2020, 2020.

Tang, M.: Abundance and fractional solubility of aerosol iron during winter at a coastal city in northern China: similarities and contrasts between fine and coarse particles, Zenodo [data set], https://doi.org/10.5281/zenodo.5774638, 2021.

Tang, S., Li, F., Lv, J., Liu, L., Wu, G., Wang, Y., Yu, W., Wang, Y., and Jiang, G.: Unexpected molecular diversity of brown carbon formed by Maillard-like reactions in aqueous aerosols, Chem. Sci., 13, 8401–8411, https://doi.org/10.1039/d2sc02857c, 2022.

van Pinxteren, D., Plewka, A., Hofmann, D., Müller, K., Kramberger, H., Svrcina, B., Bächmann, K., Jaeschke, W., Mertes, S., Collett, J. L., and Herrmann, H.: Schmücke hill cap cloud and valley stations aerosol characterisation during FEBUKO (II): Organic compounds, Atmos. Environ., 39, 4305–4320, https://doi.org/10.1016/j.atmosenv.2005.02.014, 2005.

Vidovic, K., Lasic Jurkovic, D., Sala, M., Kroflic, A., and Grgic, I.: Nighttime Aqueous-Phase Formation of Nitrocatechols in the Atmospheric Condensed Phase, Environ. Sci. Technol., 52, 9722–9730, https://doi.org/10.1021/acs.est.8b01161, 2018.

Vione, D., Maurino, V., Minero, C., and Ezio, P.: Aqueous Atmospheric Chemistry: Formation of 2,4-Dinitrophenol upon Nitration of 2-Nitrophenol and 4-Nitrophenol in Solution, Environ. Sci. Technol., 39, 7921–7931, https://doi.org/10.1021/es050824m 2005.

Wang, L., Wang, X., Gu, R., Wang, H., Yao, L., Wen, L., Zhu, F., Wang, W., Xue, L., Yang, L., Lu, K., Chen, J., Wang, T., Zhang, Y., and Wang, W.: Observations of fine particulate nitrated phenols in four sites in northern China: concentrations, source apportionment, and secondary formation, Atmos. Chem. Phys., 18, 4349–4359, https://doi.org/10.5194/acp-18-4349-2018, 2018.

Wang, Y., Hu, M., Lin, P., Tan, T., Li, M., Xu, N., Zheng, J., Du, Z., Qin, Y., Wu, Y., Lu, S., Song, Y., Wu, Z., Guo, S., Zeng, L., Huang, X., and He, L.: Enhancement in Particulate Organic Nitrogen and Light Absorption of Humic-Like Substances over Tibetan Plateau Due to Long-Range Transported Biomass Burning Emissions, Environ. Sci. Technol., 53, 14222–14232, https://doi.org/10.1021/acs.est.9b06152, 2019.

Wu, X., Vu, T. V., Shi, Z., Harrison, R. M., Liu, D., and Cen, K.: Characterization and source apportionment of carbonaceous $PM_{2.5}$ particles in China – A review, Atmos. Environ., 189, 187–212, https://doi.org/10.1016/j.atmosenv.2018.06.025, 2018.

Xu, W., Han, T., Du, W., Wang, Q., Chen, C., Zhao, J., Zhang, Y., Li, J., Fu, P., Wang, Z., Worsnop, D. R., and Sun, Y.: Effects of Aqueous-Phase and Photochemical Pro-

cessing on Secondary Organic Aerosol Formation and Evolution in Beijing, China, Environ. Sci. Technol., 51, 762–770, https://doi.org/10.1021/acs.est.6b04498, 2017.

Yang, L., Huang, R. J., Shen, J., Wang, T., Gong, Y., Yuan, W., Liu, Y., Huang, H., You, Q., Huang, D. D., and Huang, C.: New Insights into the Brown Carbon Chromophores and Formation Pathways for Aqueous Reactions of alpha-Dicarbonyls with Amines and Ammonium, Environ. Sci. Technol., 57, 12351–12361, https://doi.org/10.1021/acs.est.3c04133, 2023.

Yang, L., Huang, R. J., Yuan, W., Huang, D. D., and Huang, C.: pH-Dependent Aqueous-Phase Brown Carbon Formation: Rate Constants and Implications for Solar Absorption and Atmospheric Photochemistry, Environ. Sci. Technol., 58, 1236–1243, https://doi.org/10.1021/acs.est.3c07631, 2024.

Yang, Z., Tsona, N. T., George, C., and Du, L.: Nitrogen-Containing Compounds Enhance Light Absorption of Aromatic-Derived Brown Carbon, Environ. Sci. Technol., 56, 4005–4016, https://doi.org/10.1021/acs.est.1c08794, 2022.

Zhang, H., Li, R., Dong, S., Wang, F., Zhu, Y., Meng, H., Huang, C., Ren, Y., Wang, X., Hu, X., Li, T., Peng, C., Zhang, G., Xue, L., Wang, X., and Tang, M.: Abundance and Fractional Solubility of Aerosol Iron During Winter at a Coastal City in Northern China: Similarities and Contrasts Between Fine and Coarse Particles, J. Geophys. Res. Atmos., 127, e2021JD036070, https://doi.org/10.1029/2021jd036070, 2021.